Local and global consequences of reward-evoked striatal dopamine release

https://doi.org/10.1038/s41586-020-2158-3

Received: 13 February 2019

Accepted: 29 January 2020

Published online: 1 April 2020

Check for updates

Nan Li[1] & Alan Jasanoff[1,2,3]✉

The neurotransmitter dopamine is required for the reinforcement of actions by rewarding stimuli[1]. Neuroscientists have tried to define the functions of dopamine in concise conceptual terms[2], but the practical implications of dopamine release depend on its diverse brain-wide consequences. Although molecular and cellular effects of dopaminergic signalling have been extensively studied[3], the effects of dopamine on larger-scale neural activity profiles are less well-understood. Here we combine dynamic dopamine-sensitive molecular imaging[4] and functional magnetic resonance imaging to determine how striatal dopamine release shapes local and global responses to rewarding stimulation in rat brains. We find that dopamine consistently alters the duration, but not the magnitude, of stimulus responses across much of the striatum, via quantifiable postsynaptic effects that vary across subregions. Striatal dopamine release also potentiates a network of distal responses, which we delineate using neurochemically dependent functional connectivity analyses. Hot spots of dopaminergic drive notably include cortical regions that are associated with both limbic and motor function. Our results reveal distinct neuromodulatory actions of striatal dopamine that extend well beyond its sites of peak release, and that result in enhanced activation of remote neural populations necessary for the performance of motivated actions. Our findings also suggest brain-wide biomarkers of dopaminergic function and could provide a basis for the improved interpretation of neuroimaging results that are relevant to learning and addiction.

To permit combined functional magnetic resonance imaging (fMRI) and molecular neuroimaging of dopamine during phasic reward signalling, we implanted rats with cannulae targeting the ventral striatum and electrodes targeting the lateral hypothalamus (LH) (Fig. 1a), a structure that contains neurochemically diverse fibres that provide robust behavioural reinforcement when stimulated[5]. We tested the rats for self-stimulation (Extended Data Fig. 1), lightly sedated them and placed them in a 9.4-Tesla magnetic resonance imaging (MRI) scanner. Scanning was performed during and after pre-infusion of a dopamine-sensitive protein-based MRI contrast agent, BM3h-9D7 (9D7)[6], followed by LH stimulation. A multi-gradient echo MRI pulse sequence was used for readout[7], providing simultaneous indication of T_1-weighted MRI contrast that arises from the dopamine sensor, along with blood-oxygen-level-dependent (BOLD) contrast that reflects neural population activity (Fig. 1b, Extended Data Fig. 2a).

Selectivity of the sensor-mediated responses was verified by comparing the T_1-weighted signal in the presence of 9D7 with equivalent data from separate rats that were injected with a control contrast agent, BM3h-WT, which lacks dopamine sensitivity[8] (Fig. 1c). Although haemodynamic responses are largely suppressed in the presence of either agent (Extended Data Fig. 2b, c), comparison of the MRI signals mediated by 9D7 and BM3h-WT also enables the identification of slow residual haemodynamic signals that are present in the T_1-weighted time courses (Fig. 1d). These residual signals could be removed by voxel-level baseline correction using either the mean BM3h-WT response or the echo time-dependent component of the 9D7 response (Extended Data Fig. 3).

We determined a map of peak stimulus-dependent dopamine release for a region infused with 9D7, which encompassed the nucleus accumbens (NAc), medial caudate putamen (CPu), olfactory tubercle (Tu) and lateral septal area (LS) (Fig. 2a). Voxel-level dopamine concentrations were derived from MRI data from five rats using a signal modelling approach[4] (Extended Data Fig. 4a, Methods). The absence of dopamine-independent signals was confirmed in data obtained using the BM3h-WT control agent (Extended Data Fig. 4b, c). Statistical analysis (Extended Data Fig. 4d, e) corroborates spatial features of the 9D7-dependent profile. We also obtained a corresponding striatal map of BOLD fMRI responses to LH stimulation[9,10] (Fig. 2b); a separate group of five uninjected rats was used for this experiment, to avoid the attenuating effects of the contrast agent on haemodynamic signals (Fig. 1, Extended Data Fig. 2).

Reward-related striatal BOLD responses have previously been thought to represent dopaminergic activity[11], but a comparison of the BOLD and dopamine data in our experiments reveals notable differences. Although widespread signals are apparent in both imaging modalities, the ratio of the two signal magnitudes varies substantially among subregions (Fig. 2c). Average dopamine amplitudes are about twice as high in the NAc and medial CPu, compared with Tu and LS,

[1]Department of Biological Engineering, Massachusetts Institute of Technology, Cambridge, MA, USA. [2]Department of Brain and Cognitive Sciences, Massachusetts Institute of Technology, Cambridge, MA, USA. [3]Department of Nuclear Science and Engineering, Massachusetts Institute of Technology, Cambridge, MA, USA. ✉e-mail: jasanoff@mit.edu

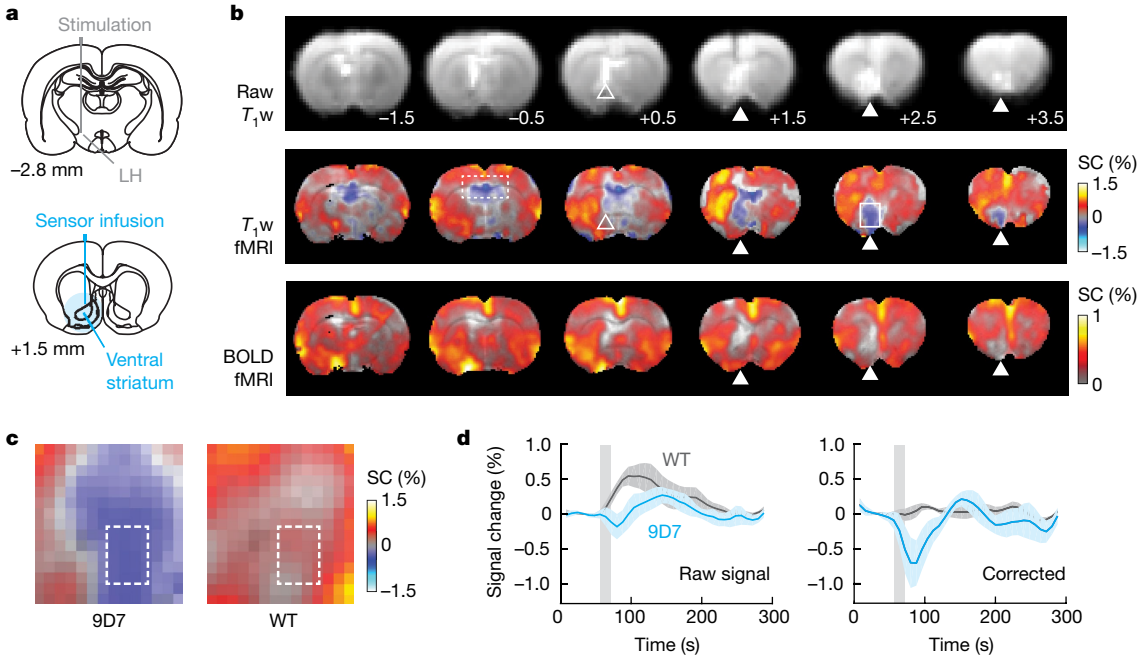

Fig. 1 | Functional and molecular imaging of responses to rewarding stimulation. a, Stimulation and contrast agent infusion sites (bregma coordinates are indicated). Stimulation electrodes (grey) are targeted to LH and ipsilateral cannulae (cyan) are targeted to ventral striatum. **b**, Simultaneous T_1-weighted (T_1w) and BOLD fMRI data collection. Top, raw T_1-weighted signal (bregma coordinates are shown). Middle, T_1-weighted fMRI signal change evoked by LH stimulation. Bottom, BOLD fMRI signal estimated from multi-echo data. Areas of peak contrast agent infusion (filled arrowheads) correspond to negative T_1-weighted fMRI signal change and suppression of haemodynamic contrast (Extended Data Fig. 2). Negative T_1-weighted fMRI signals do not colocalize with raw T_1-weighted enhancement in lateral ventricles (open arrowheads), but do occur near the corpus callosum (dashed box) in both 9D7-injected and uninjected rats (Extended Data Fig. 2a). **c**, Close-up of solid boxed region in **b**, comparing negative signal change mediated by the 9D7 dopamine sensor to the neutral effect of the wild-type control protein. **d**, Mean time courses of 9D7 (cyan) and BM3h-WT (grey) responses evoked by LH stimulation (grey bar), evaluated over the boxed regions in **c**, before (left) and after (right) correction for residual haemodynamic responses. Shading depicts s.e.m. from $n = 5$ rats.

whereas BOLD responses vary by less than 15% of the mean amplitude among striatal regions of interest (ROIs) (Fig. 2d, e).

Dopamine and haemodynamic fMRI responses also differ temporally and as a function of stimulus strength (Fig. 2f, g). Amperometry recordings show that dopamine dynamics track stimulation blocks with a full width at half maximum of about 20 s (Extended Data Fig. 5a). Dopamine-dependent MRI responses exhibit broadening due to the influence of sensor kinetics (Extended Data Fig. 5b, c), but occur on a similar time scale and track the predicted total dopamine levels with high fidelity. The full width at half maximum of dopamine responses averages 40 ± 6 s over the region in which peak responses were observed; the mean response amplitude in this area rises approximately linearly with stimulation frequency (Fig. 2h). By contrast, the BOLD response extends for about 200 s following stimulus offset; the full width at half maximum reaches 84 ± 8 s, significantly longer than the dopamine response (t-test $P < 0.0001$, $n = 5$ rats). The amplitude of the BOLD responses also saturates with increasing LH stimulus strength. Relative to responses at 120-Hz stimulation, dopamine amplitudes at 200-Hz stimulation are 50% higher (significant difference; t-test $P = 0.03$, $n = 5$ rats) whereas BOLD responses are virtually the same (t-test $P = 0.58$, $n = 5$ rats).

Discrepancies between striatal dopamine and BOLD signals could arise from non-dopaminergic activity[12] or from postsynaptic contributions of dopamine to BOLD responses. To evaluate these possibilities, we performed a second set of haemodynamic fMRI experiments before and after systemic injection of a combination of SCH 23390 and eticlopride, antagonists of the dopamine D1 and D2 receptors, respectively (Fig. 3a). Treatment with this cocktail improves voxel-level correlation between dopamine and BOLD responses throughout much of the medial striatum (Fig. 3b). Seventy-seven per cent of voxels show increased correlation between dopamine and BOLD signals after inhibition, and 10% of voxels show a significant improvement ($\Delta Z > 2.0$, $P < 0.05$) at an individual level. This suggests that the postsynaptic effects of dopamine contribute substantially to differences between the response profiles presented in Fig. 2.

Inhibition of dopamine receptors also increases the topographic similarity of the dopamine and BOLD amplitude maps, as reflected by a reduction in the deviation from direct proportionality of dopamine and BOLD response magnitudes across all voxels in the field of view (Extended Data Fig. 6a). The root mean squared deviation from proportionality decreases by 25% after blockade of the D1 and D2 receptors (significant with F-test $P = 0.0019$); this coincides with an increase in the correlation coefficient between dopamine and BOLD responses, from −0.16 (significant with $P = 0.001$) before dopamine receptor inhibition to 0.01 ($P = 0.8$) afterwards. Improvements by 23–44% in the proportionality between dopamine and BOLD responses are also significant within subregions (F-tests $P \leq 0.005$) (Fig. 3c).

These effects arise in part from dopamine-receptor-dependent changes in BOLD fMRI response amplitudes. In the presence of blockers, the distribution of voxelwise BOLD amplitudes is significantly lower in the medial CPu, LS and Tu (19–33% changes, paired t-test $P \leq 0.05$), but not in the NAc (8% change, $P = 0.13$) (Fig. 3d). More notable, however, is the effect of dopamine receptor inhibition on fMRI time courses in the striatum. All ROIs experience substantial decreases in response duration (significant with t-test $P \leq 0.04$) (Fig. 3e), resulting in values that are comparable to the dopamine release time courses themselves (Fig. 2f). By contrast, treatment with dopamine blockers barely changes the spatiotemporal properties of dopamine release (Extended Data Fig. 6b–d), indicating that feedback onto dopamine itself does not have a substantial role.

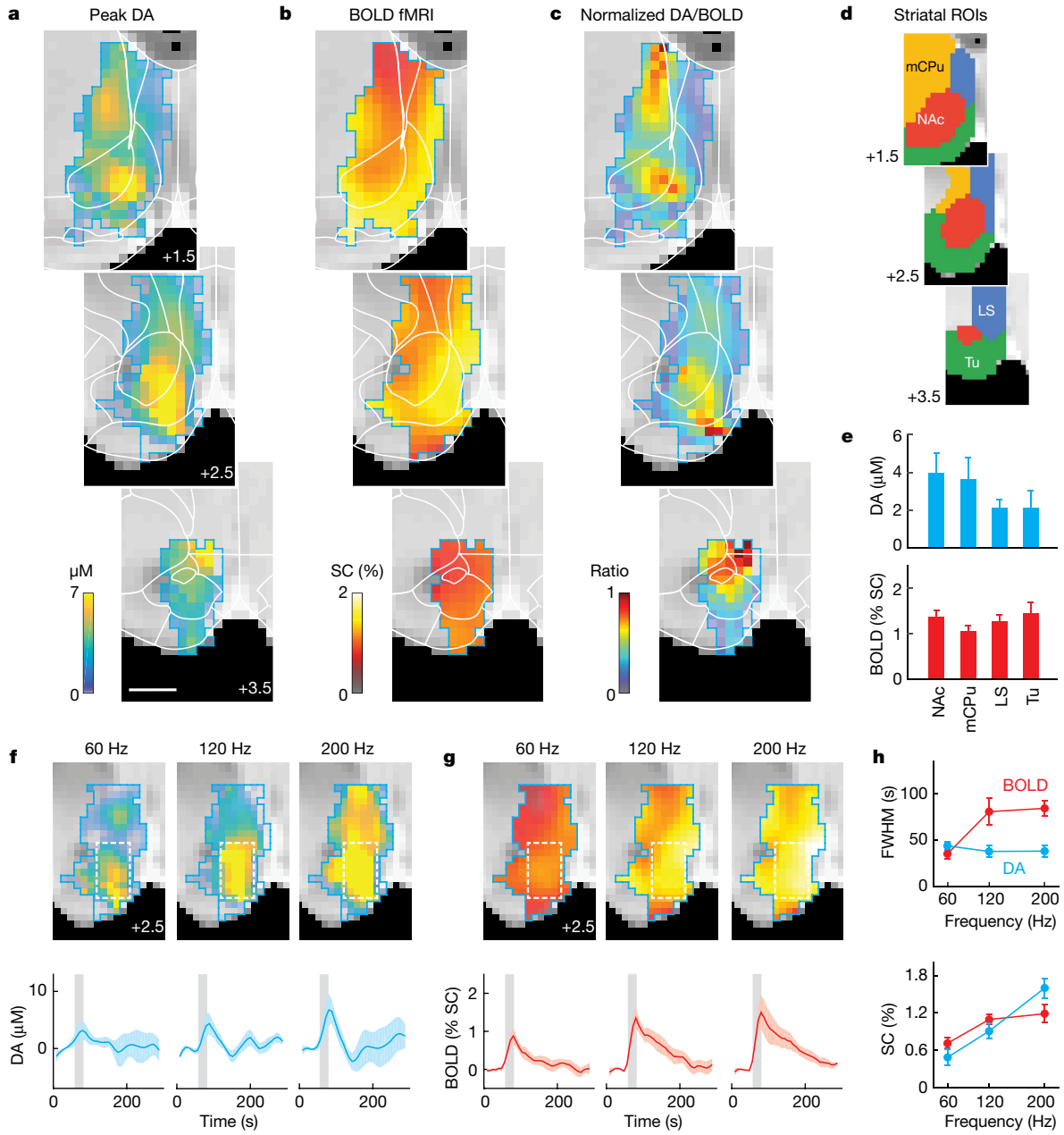

Fig. 2 | Dissociable profiles of reward-evoked striatal dopamine release and BOLD activation. a, Peak concentrations of dopamine release (DA) evoked by rewarding stimulation (colour), averaged over sensor infused regions from five rats (cyan outline). Scale bar, 1 mm. **b**, Amplitudes of the BOLD fMRI signal evoked by LH stimulation, in the region infused by the contrast agent, as shown in **a**. **c**, Normalized ratio of profiles in **a** and **b**, indicating the lack of spatial correspondence between dopamine and BOLD. **d**, Definition of striatal subregions in medial CPu (mCPu), NAc, LS and Tu. **e**, ROI-averaged dopamine amplitudes (cyan) and BOLD signal changes (red) in each striatal subregion. Error bars indicate s.e.m. of five rats. **f**, Maps of the amplitude of dopamine release (top) as a function of the indicated rewarding stimulus frequency, with corresponding time courses for the dashed region shown (bottom). Shading indicates s.e.m. ($n = 5$ rats). **g**, BOLD response profiles shown as a function of the indicated stimulus frequency (top), with corresponding time courses (bottom). **h**, Frequency dependence of full width at half maximum (FWHM) (top) and per cent signal change (%SC) (bottom) for dopamine (cyan) and BOLD (red) responses to rewarding stimulation. The s.e.m. of $n = 5$ rats is indicated.

Taken together, these results indicate that the postsynaptic effects of dopamine contribute significantly to the discrepancy between striatal BOLD fMRI and dopamine signals elicited by rewarding stimulation, and that reward-evoked striatal fMRI signals cannot be explained in terms of input alone[13]. By comparing the D1 and D2 inhibitor-dependent changes in BOLD signal with the dopamine imaging data shown in Fig. 1, we determined a spatiotemporal impulse response function that describes the net effects of dopamine at each voxel (Fig. 3f) and in each striatal ROI (Fig. 3g). This analysis suggests that the primary effect of dopamine is to modulate the duration of fMRI-detectable responses to stimulation. The effects of dopamine on the magnitude of brain activation appear to be subtler and more variable across striatal subregions, perhaps because of regional differences in receptor densities and occupancies[14].

We hypothesized that long-range consequences of striatal dopamine release could be discovered by identifying brain-wide fMRI signals that correlate with the dopamine response characteristics. BOLD fMRI data obtained from rats that were not treated with contrast agent show that rewarding stimulation evokes activation in structures throughout the rostral half of the brain (Fig. 4a). To locate responses that might be

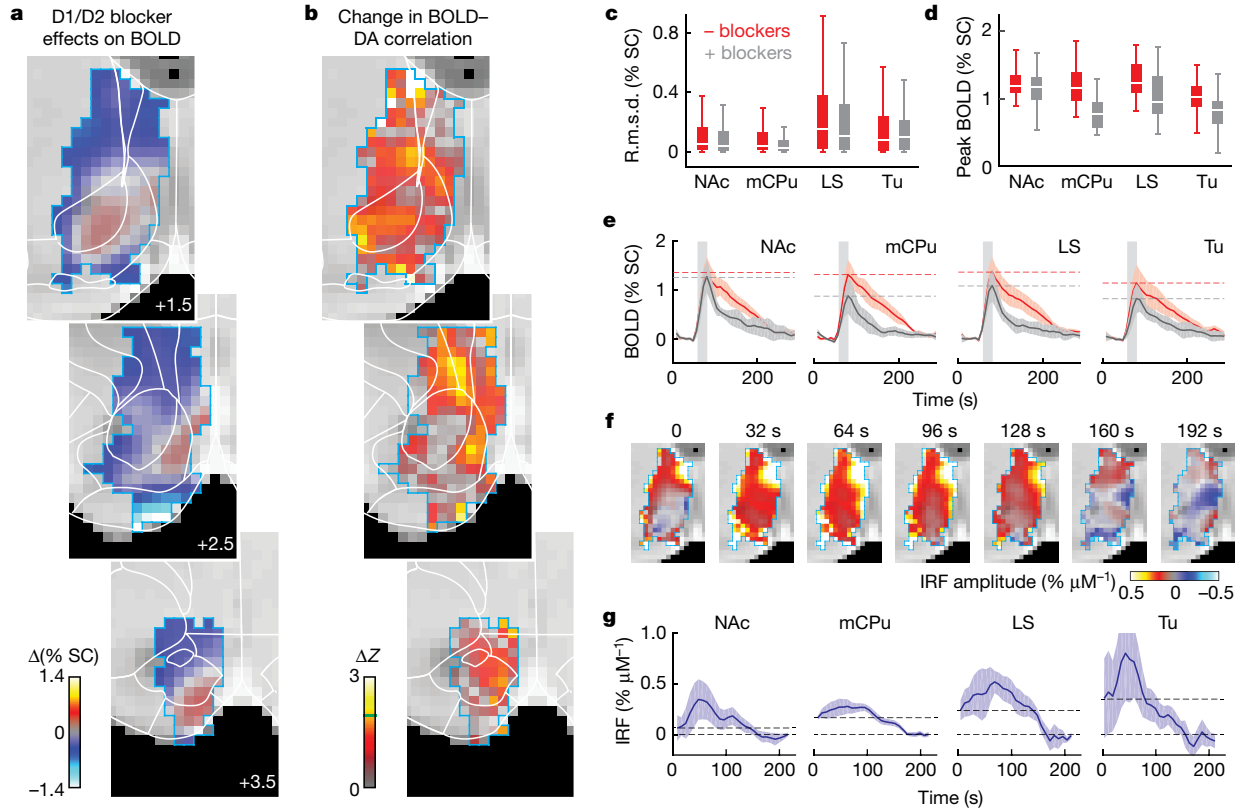

Fig. 3 | Dopamine-dependent modulation of striatal fMRI signals. a, Change in BOLD signal amplitude (Δ(% SC)) in response to rewarding stimulation upon addition of D1 and D2 dopamine receptor inhibitors; data shown for the region of Fig. 2 infused with the contrast agent (cyan outline). **b**, Change in *Z* value (Δ*Z*) for correlation between striatal BOLD and dopamine signals upon addition of D1 and D2 blockers. Increased correlation is statistically significant at an individual voxel level for $\Delta Z \geq 2.0$ (green line in colour scale). **c**, Root mean squared deviation (r.m.s.d.) from direct proportionality between dopamine and BOLD response magnitudes across voxels in striatal subregions, before (red) and after (grey) treatment with D1 and D2 inhibitors. Boxes denote median (centre line), first and third quartiles (box edges), and full range of values (whiskers) in each ROI (outliers are not shown). Striatal subfields include NAc, medial CPu (mCPu), LS and Tu. **d**, Peak fMRI response to rewarding stimulation in the absence (red) and presence (grey) of dopamine receptor blockers. Boxes defined as in **c**. **e**, Mean BOLD response to rewarding stimulation (vertical grey bar) in each striatal subregion, before (red) and after (grey) treatment with dopamine inhibitors. Dashed lines denote peak amplitudes. Shading represents s.e.m. of $n = 5$ rats. **f**, Spatially resolved impulse response function (IRF) describing the effect of dopamine on the BOLD fMRI signal at multiple time points. **g**, Mean dopamine-dependent IRFs measured from striatal subregions. Shading denotes s.e.m. of $n = 5$ rats. Dashed lines indicate the instantaneous effect of dopamine on BOLD amplitudes (IRF at the 0 s time point).

particularly closely related to striatal dopamine, we first computed the average time course of the fMRI signal of each voxel at each stimulus strength. We then applied voxelwise multiple regression analysis using the mean striatal dopamine time courses at each stimulus strength (Fig. 2f) and the global BOLD signal as regressors; the fraction of preferentially dopamine-tracking variance was quantified at each position (Fig. 4a, middle row). At an ROI level (Fig. 4b, Extended Data Fig. 7), this analysis reveals particularly strong dopamine-tracking behaviour by BOLD signals in the CPu, motor cortex (MCx), insular cortex (ICx), secondary somatosensory cortex (S2) and LH (*Z*-test $P \leq 0.05$, $n = 5$ rats). Lesser or negligible dopamine tracking is observed in NAc, Tu, LS, cingulate cortex and ventral pallidum (*Z*-test $P \geq 0.05$, $n = 5$ rats), despite the fact that stimuli evoke comparable BOLD amplitudes in these regions.

Notably, most regions with strongly dopamine-tracking fMRI signals also display a high sensitivity to blockade of D1 and D2 receptors during stimulation (Fig. 4a, bottom), providing additional support for a connection between these regions and dopaminergic function. Strong and consistent blocker-dependent suppression of BOLD signals is observed in the CPu, MCx, ICx and S2 (before versus after *t*-test $P \leq 0.0001$) (Fig. 4b). Weaker sensitivity to D1 and D2 blockers is observed in Tu ($P = 0.047$), which does not exhibit strong dopamine tracking in the regression analysis; negligible effects ($P \geq 0.09$) are seen in LS, cingulate cortex, ventral pallidum, NAc and LH. A similar profile of fMRI signal changes is observed upon infusion of D1 and D2 inhibitors into cerebrospinal fluid, suggesting that blocker-dependent difference signals do not reflect systemic changes (Extended Data Fig. 8). The dopamine blocker and dopamine-tracking effects in MCx, ICx and S2 seem surprising, given that these cortical regions receive relatively sparse presynaptic dopamine input[15,16]. This raises the possibility that striatal dopamine indirectly modulates reward-evoked activation in the cortex, and could help to explain evidence that links the MCx and ICx in particular to reward-related functions[17,18].

We reasoned that if striatal dopamine release were causally related to distal BOLD responses, then variation of striatal-dopamine release profiles across rats would correlate with variations in distal BOLD signals. We tested this idea by using the mean BOLD responses in each ROI as components of a regression analysis of dopamine responses measured simultaneously within individual rats. Figure 4c displays the extent to which striatal dopamine signals track BOLD responses in the CPu, MCx, ICx, S2 and LH, across five rats; Fig. 4d diagrams the corresponding results averaged over each striatal subregion. These data indicate that the MCx, ICx and S2 signals do in fact correspond closely to striatal dopamine (Fig. 4d), especially in the NAc and medial CPu (regression coefficients ≥ 0.12, *t*-test $P \leq 0.045$). By contrast, BOLD signals in LH and lateral CPu (which omits 9D7-infused regions) do not correspond to dopamine measurements from striatal ROIs.

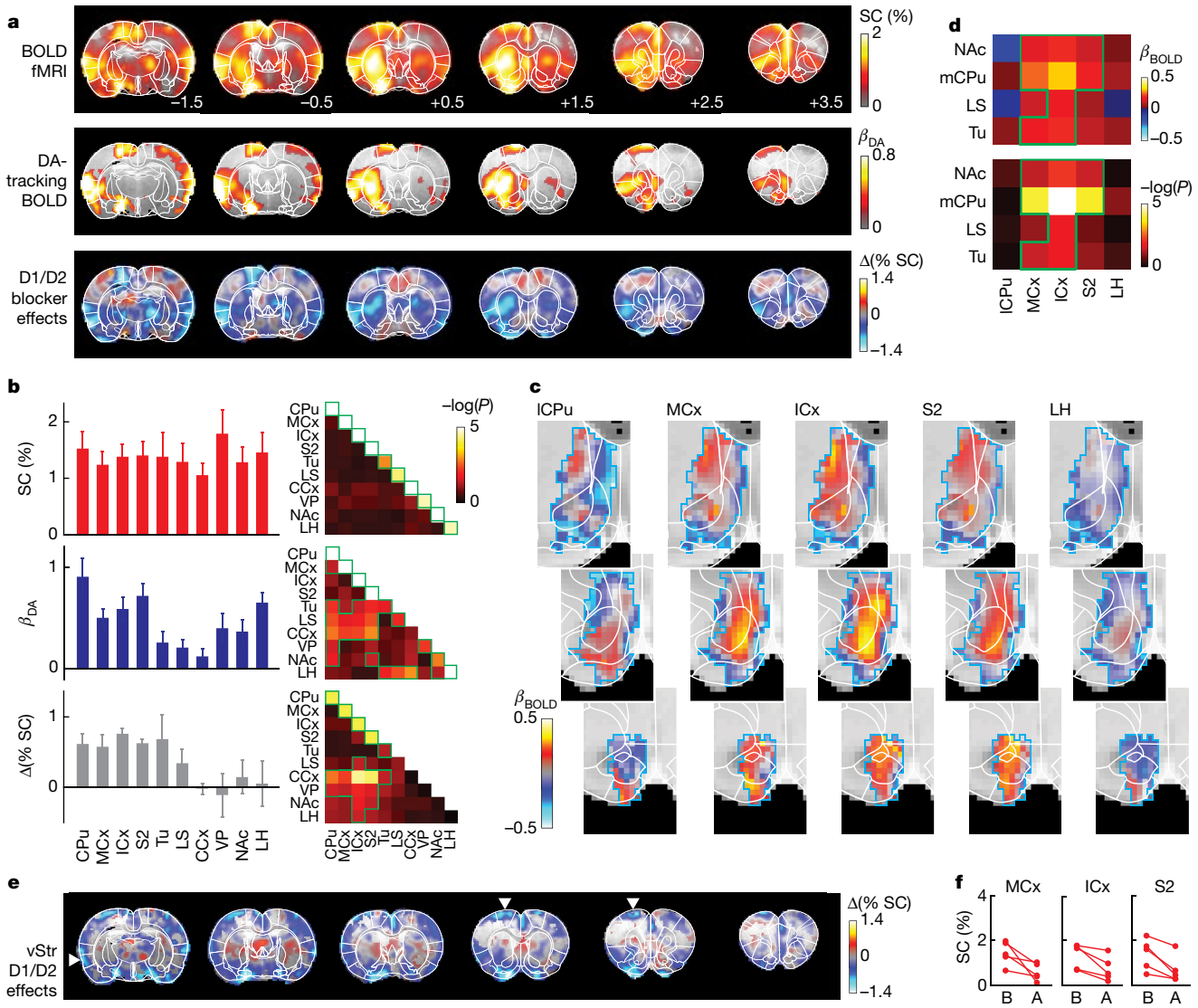

Fig. 4 | Brain-wide consequences of striatal dopamine release evoked by rewards. a, Comparison of brain-wide BOLD fMRI responses to LH stimulation (SC (%)) (top), dopamine time course-tracking components (β_{DA}) (middle) and modulation of fMRI amplitudes by systemic treatment with D1 and D2 blockers (Δ(% SC)) (bottom). Atlas divisions and bregma coordinates are indicated. Colour overlays are masked to display voxels with significant responses ($P \leq 10^{-5}$, top and bottom) or tracking ($P \leq 0.05$, middle). **b**, Mean BOLD amplitudes (top), dopamine tracking components (middle) and D1 and D2 blocker-dependent fMRI modulations (bottom) averaged over ROIs. All error bars denote s.e.m. of $n = 5$ rats. Matrices on the right specify the *t*-test *P* values for individual ROIs (diagonal) and differences between ROIs (off-diagonal); values with $P \leq 0.05$ are outlined in green. CCx, cingulate cortex; VP, ventral pallidum. **c**, Correspondence between simultaneously acquired striatal dopamine and distal fMRI responses from five regions, computed by linear regression of the dopamine signal to yield maps of BOLD-tracking amplitudes (β_{BOLD}). The lateral CPu region (lCPu) excludes 9D7-infused CPu areas. **d**, ROI averages of data in **c**, presented as mean β_{BOLD} values (top) with corresponding *t*-test *P* values for significance (bottom) between striatal subregions (vertical axis) and distal BOLD signals (horizontal axis). Values with $P \leq 0.05$ are outlined in green. **e**, Modulation of fMRI signals produced by ventral striatal (vStr) infusion of D1 and D2 blockers. Arrowheads highlight similarity with results of **b**. **f**, Consistent long-range effects of striatal dopamine inhibition in MCx, ICx and secondary somatosensory cortex; the differences before (B) versus after (A) treatment are significant with paired *t*-test $P \leq 0.05$, $n = 5$ rats.

Importantly, this correspondence between striatal dopamine release and distal BOLD signals observed across individual rats is sharply reduced in the presence of D1 and D2 blockers (Extended Data Fig. 9), further implying a causal role for dopamine in the observed effects.

As an additional test of the relationship between striatal dopamine and cortical BOLD responses, we infused SCH 23390 and eticlopride locally into the ventral striatum and examined their effects on activation induced by stimulation of LH. As with the global inhibition experiment shown in Fig. 4a, this experiment also reveals substantial peaks of difference signal in cortical regions, confirming that striatal dopaminergic signalling contributes to the modulation of distal BOLD signals (Fig. 4e, Extended Data Fig. 10a). Peak responses in the MCx, ICx and S2 are 0.6–0.9% lower on average in the presence of striatal dopamine receptor inhibitors that in their absence (significant with paired *t*-test $P \leq 0.05$) (Fig. 4f). Similar results were obtained using striatal infusions that also contained the α2 adrenergic inhibitor yohimbine (Extended Data Fig. 10b), supporting the dopamine specificity of these findings and suggesting that α2 agonism by medotomidine does not alter the outcome.

A straightforward interpretation of these results is that feedforward effects of phasic dopamine release in the NAc and medial CPu causally modulate fMRI responses in the distal cortical regions[19]. The fact that LH and CPu show strong dopamine tracking in Fig. 4b suggests that these regions receive input that temporally parallels, but does not depend

on, ventral striatal dopamine release. The fact that LH is not sensitive to systemic inhibition of D1 and D2 receptors implies that activation of this region is mediated by nondopaminergic mechanisms[20], consistent with weak hypothalamic responses reported upon stimulation of D1- and D2-expressing striatal neurons[21]. These findings do not rule out additional roles for non-striatal dopamine or non-dopaminergic mechanisms.

Considered together, our results are notable in several respects. First, they explicitly link striatal dopamine release to a constellation of brain responses that could be mechanistically important for reward-related behaviours. Topographic features could be characterized as a result of our imaging approach, and functional connectivity results were strengthened by mapping dopamine and BOLD simultaneously within individual rats. Effective connectivity between striatal dopamine domains and diverse brain regions, including MCx and ICx, suggests a basis for the multifaceted contributions of dopamine to motivated action. Second, our results show how dopamine modulates neural response profiles in ways that go beyond simple excitation or inhibition[22], contrasting with fMRI-based reports that link optogenetic stimulation of dopaminergic neurons primarily to increases in postsynaptic activity[23,24]. The dopamine-dependent enhancement of striatal response durations we observe could reflect action of dopaminergic signalling cascades involved in plasticity and learning[25,26]. Third, our findings could help to explain other neuroimaging results related to dopamine or reward. For instance, our dissociation of dopamine and fMRI signals in the ventral striatum could account for deviations of striatal BOLD responses from predictions of temporal difference learning theory in people[27]. Furthermore, correlates of striatal dopamine release we have identified could provide new biomarkers for assessing dopaminergic function.

Online content

Any methods, additional references, Nature Research reporting summaries, source data, extended data, supplementary information, acknowledgements, peer review information; details of author contributions and competing interests; and statements of data and code availability are available at https://doi.org/10.1038/s41586-020-2158-3.

1. Wise, R. A. Dopamine, learning and motivation. *Nat. Rev. Neurosci*. **5**, 483–494 (2004).
2. Berke, J. D. What does dopamine mean? *Nat. Neurosci*. **21**, 787–793 (2018).
3. Bamford, N. S., Wightman, R. M. & Sulzer, D. Dopamine's effects on corticostriatal synapses during reward-based behaviors. *Neuron* **97**, 494–510 (2018).
4. Lee, T., Cai, L. X., Lelyveld, V. S., Hai, A. & Jasanoff, A. Molecular-level functional magnetic resonance imaging of dopaminergic signaling. *Science* **344**, 533–535 (2014).
5. Olds, J. & Milner, P. Positive reinforcement produced by electrical stimulation of septal area and other regions of rat brain. *J. Comp. Physiol. Psychol*. **47**, 419–427 (1954).
6. Brustad, E. M. et al. Structure-guided directed evolution of highly selective p450-based magnetic resonance imaging sensors for dopamine and serotonin. *J. Mol. Biol*. **422**, 245–262 (2012).
7. Kundu, P. et al. Integrated strategy for improving functional connectivity mapping using multiecho fMRI. *Proc. Natl Acad. Sci. USA* **110**, 16187–16192 (2013).
8. Shapiro, M. G. et al. Directed evolution of a magnetic resonance imaging contrast agent for noninvasive imaging of dopamine. *Nat. Biotechnol*. **28**, 264–270 (2010).
9. Krautwald, K., Min, H. K., Lee, K. H. & Angenstein, F. Synchronized electrical stimulation of the rat medial forebrain bundle and perforant pathway generates an additive BOLD response in the nucleus accumbens and prefrontal cortex. *Neuroimage* **77**, 14–25 (2013).
10. Fiallos, A. M. et al. Reward magnitude tracking by neural populations in ventral striatum. *Neuroimage* **146**, 1003–1015 (2017).
11. O'Doherty, J. P., Dayan, P., Friston, K., Critchley, H. & Dolan, R. J. Temporal difference models and reward-related learning in the human brain. *Neuron* **38**, 329–337 (2003).
12. Brocka, M. et al. Contributions of dopaminergic and non-dopaminergic neurons to VTA-stimulation induced neurovascular responses in brain reward circuits. *Neuroimage* **177**, 88–97 (2018).
13. Logothetis, N. K. The neural basis of the blood-oxygen-level-dependent functional magnetic resonance imaging signal. *Phil. Trans. R. Soc. Lond. B* **357**, 1003–1037 (2002).
14. Mandeville, J. B. et al. A receptor-based model for dopamine-induced fMRI signal. *Neuroimage* **75**, 46–57 (2013).
15. Boja, J. W. et al. High-affinity binding of [^{125}I]RTI-55 to dopamine and serotonin transporters in rat brain. *Synapse* **12**, 27–36 (1992).
16. Freed, C. et al. Dopamine transporter immunoreactivity in rat brain. *J. Comp. Neurol*. **359**, 340–349 (1995).
17. Kapogiannis, D., Campion, P., Grafman, J. & Wassermann, E. M. Reward-related activity in the human motor cortex. *Eur. J. Neurosci*. **27**, 1836–1842 (2008).
18. Naqvi, N. H. & Bechara, A. The hidden island of addiction: the insula. *Trends Neurosci*. **32**, 56–67 (2009).
19. Arsenault, J. T., Nelissen, K., Jarraya, B. & Vanduffel, W. Dopaminergic reward signals selectively decrease fMRI activity in primate visual cortex. *Neuron* **77**, 1174–1186 (2013).
20. Stuber, G. D. & Wise, R. A. Lateral hypothalamic circuits for feeding and reward. *Nat. Neurosci*. **19**, 198–205 (2016).
21. Lee, H. J. et al. Activation of direct and indirect pathway medium spiny neurons drives distinct brain-wide responses. *Neuron* **91**, 412–424 (2016).
22. Tritsch, N. X. & Sabatini, B. L. Dopaminergic modulation of synaptic transmission in cortex and striatum. *Neuron* **76**, 33–50 (2012).
23. Ferenczi, E. A. et al. Prefrontal cortical regulation of brainwide circuit dynamics and reward-related behavior. *Science* **351**, aac9698 (2016).
24. Decot, H. K. et al. Coordination of brain-wide activity dynamics by dopaminergic neurons. *Neuropsychopharmacology* **42**, 615–627 (2017).
25. Nakano, T., Doi, T., Yoshimoto, J. & Doya, K. A kinetic model of dopamine- and calcium-dependent striatal synaptic plasticity. *PLOS Comput. Biol*. **6**, e1000670 (2010).
26. Gerfen, C. R. & Surmeier, D. J. Modulation of striatal projection systems by dopamine. *Annu. Rev. Neurosci*. **34**, 441–466 (2011).
27. Klein-Flügge, M. C., Hunt, L. T., Bach, D. R., Dolan, R. J. & Behrens, T. E. Dissociable reward and timing signals in human midbrain and ventral striatum. *Neuron* **72**, 654–664 (2011).

Methods

Sample sizes for rat experiments were chosen to ensure reproducibility and quantify observed effects, rather than to guarantee recognition of prespecified effect sizes with a given level of power. Experiments were not randomized or blinded.

Rats

Male Sprague-Dawley rats (300–350 g) were purchased from Charles River Laboratories. The rats were housed and maintained on a 12 h light/dark cycle with ad libitum access to food and water. All rat procedures were performed in strict compliance with the Massachusetts Institute of Technology Committee on Animal Care oversight, and in accordance with the institutional and National Institutes of Health guidelines.

Preparation of MRI contrast agents

Wild-type (WT) and 9D7 variants of the cytochrome P450 BM3 haem domain (BM3h) were prepared following previously described procedures[4,6,8]. In brief, overnight cultures of *Escherichia coli* BL21(DE3) cells carrying a pCWori(+) plasmid encoding the BM3h variants regulated by a tandem Ptac promoter were inoculated at a 1:100 volumetric ratio into terrific broth (TB) medium containing carbenicillin at 100 μg/ml. The shake flask cultures were grown at 37 °C to an optical density at 600 nm in the 0.8–1.0 range, and expression was induced by addition of 0.6 mM isopropyl β-D-1-thiogalactopyranoside for 12–16 h at 30 °C in the presence of 0.6 mM δ-aminolevulinate. Collected pellets were lysed using a commercial reagent supplemented with lysozyme, benzonase and a protease inhibitor cocktail. The protein was affinity-purified from centrifugally clarified lysate using Ni-NTA agarose resin, concentrated in a 30-kDa molecular weight cut-off ultracentrifugation device, further purified by high-performance liquid chromatography, and buffer-exchanged into phosphate-buffered saline, pH 7.4, using a gel filtration desalting column. Aliquots of purified protein were flash-frozen in liquid nitrogen and stored at −80 °C. The concentrations of the BM3h variants were determined spectrophotometrically as the reduced carbon monoxide complex with molar extinction coefficient 91 mM^{-1} cm^{-1} at 450 nm.

Implantation of stimulation electrodes and cannula

Adult rats were anaesthetized with isoflurane (4% for induction, 2% for maintenance), and head-mounted on a rodent stereotaxic instrument (David Kopf Instruments), with a heating pad to keep the body temperature at 37 °C. Heart rate and blood oxygenation were continuously monitored using a pulse oximeter (Nonin Medical) during subsequent procedures. The scalp was retracted and small holes were drilled into the skull above the target sites. A bipolar stimulating electrode was lowered into the medial forebrain bundle at the level of the LH, with coordinates −2.8 mm anterioposterior, +1.7 mm mediolateral and +8.6 mm dorsoventral to bregma. An MRI-compatible 0.5-mm-long 22-gauge guide cannula (Plastics One) was lowered to the cerebral cortex above the NAc, ipsilateral to the LH stimulation electrode, at +1.5 mm anterioposterior and +1.5 mm mediolateral to bregma. A custom-fabricated plastic headpost was placed in front of the guide cannula to secure the head position to the cradle for MRI imaging. After all the items were secured on the skull, dental cement (C&B Metabond, Parkell) was applied to the entire exposed skull surface area to hold them rigidly in place. Rats were maintained under a heating pad until fully recovered, and treated with 0.3 mg/kg slow-release buprenorphine subcutaneously to minimize pain and discomfort. Rats were allowed 3–7 days for recovery before any additional experiments.

Intracranial self-stimulation tests

To assess the ability of the implanted LH electrodes to support rewarding stimulation, rats were evaluated for intracranial self-stimulation behaviour in a plexiglass operant chamber (28 × 21 × 21 cm) (Lafayette Instruments). An infrared nose poke sensor was positioned at one end of the operant chamber. Input from the sensor was recorded via a digital input–output interface (National Instruments). Each nose poke triggered a 1-s train of 0.15-mA 1-ms electrical pulses delivered to the rat with frequency of 120 Hz via its LH electrode. A minimum of 2 s was required between the onsets of successive nose-poke-triggered rewards. Intracranial self-stimulation was quantified over three 30-s trial periods in each rat before imaging. To examine the effect of striatal infusions on intracranial self-stimulation behaviour, 500 μM 9D7 ($n = 5$) or saline vehicle ($n = 3$) was infused into the ventral striatum before testing, in each case at a rate of 0.1 μl/min. Results of these tests (Extended Data Fig. 1) indicate that 9D7 infusion does not noticeably reduce the propensity of rats to self-stimulate, compared with saline treatment.

Receptor inactivation treatments

The dopamine D1 receptor antagonist SCH 23390 and the dopamine D2 receptor antagonist eticlopride (MilliporeSigma) were used together to inhibit dopamine signalling[28,29]. One group of rats received systemic treatment by intravenous injection of the antagonists with a bolus dosage of 0.4 mg/kg SCH 23390 and 0.4 mg/kg eticlopride, formulated in 0.9% sterile saline, followed by continuous infusion at 0.8 mg/kg/h of each drug. Some of these rats were used for dopamine imaging using the 9D7 sensor and some were used for BOLD imaging in the absence of contrast agent infusion. Another group of rats received locally targeted intracranial infusion of 0.13 μg/min of each drug for 10 min at 0.1 μl/min, followed by further infusion of 0.013 μg/min for a further 10 min. This injection was targeted at the NAc core area, anterioposterior +1.5mm, mediolateral +1.5mm, and dorsoventral +7 mm to bregma, via a cannula ipsilateral to the LH stimulation electrode. A third set of rats received the same striatally targeted treatment with D1 and D2 inhibitors mixed also with identical mass doses of the α2 receptor antagonist yohimbine. A fourth set of rats received 0.07 mg/kg SCH 23390 and 0.07 mg/kg eticlopride (MilliporeSigma) administered via intracerebrospinal fluid infusion into the cisterna magna at a rate of 5 μl/min over 20 min, followed by a 40-min equilibration period, before fMRI experiments. Drug doses used in the experiments were based on pilot studies and precedents in the literature[30,31].

MRI methods

Rats that performed intracranial self-stimulation behaviour effectively (>20 responses per minute) were selected for MRI experiments. To prepare them for imaging, these rats were anaesthetized initially with isoflurane (2%) and intubated via a tracheotomy; then isoflurane was discontinued and rats were sedated with an intraperitoneal bolus of 1 mg/kg medetomidine and paralyzed with pancuronium (bolus dose of 1 mg/kg, intraperitoneally) to prevent motion artefacts during experiments. Rats were ventilated with a small animal ventilator (Harvard Apparatus) which operated at 62 beats per minute with a 6-ml stroke volume, delivering oxygen and air as a 5:1 ratio mixture. Rats were warmed using a water-circulating pad. Heart rate and blood oxygenation saturation level were continuously monitored using an MRI-compatible noninvasive infrared pulse oximeter (Nonin Medical).

The rats were then fixed via their headposts into a custom-built cradle for imaging. An internal cannula connected via tubing to a 25-μl Hamilton syringe was back-filled with a 500 μM 9D7 protein solution, inserted into the guide cannula and lowered to a striatal location in the NAc (anterioposterior +1.5 mm, mediolateral +1.5 mm, dorsoventral +7 mm). Once positioned in the MRI magnet, medetomidine (1 mg/kg/h) and pancuronium (1 mg/kg/h) were delivered continuously via an intraperitoneal catheter.

All MRI images were obtained on a 9.4-T scanner (Bruker Biospin). A transmit-only 70-cm-inner-diameter linear volume coil (Bruker) and a 2-cm-diameter receive-only surface coil (Doty Scientific) were used for excitation and detection, respectively. Scanner operation was performed using the Paravision 5.1 software (Bruker). High-resolution

anatomical MRI images were acquired using a T_2-weighted rapid acquisition with refocused echoes pulse sequence with rapid acquisition with refocused echoes factor = 8, effective echo time (TE) = 30 ms, repetition time (TR) = 5 s, in-plane field of view (FOV) = 1.92 × 1.92 cm, in plane resolution 100 μm × 100 μm, and slice thickness = 1 mm for 6 coronal slices.

For functional imaging of dopamine, the 9D7 sensor protein (500 μM) was delivered to the brain by intracranial microinjection through the cannula with a infusion rate of 0.1 μl/min. The sensor was continuously infused for about 50 min, and a series of T_1-weighted fast low angle shot MRI images were acquired to evaluate the spread of the contrast agent in the brain. Imaging was then continued in conjunction with LH stimulation, to discern functional and molecular responses. These image series were acquired using a multi-gradient echo pulse sequence with bandwidth = 200 kHz, TE = 4, 12, and 20 ms, flip angle 30°, TR = 251.9 ms, scan time = 8 s, FOV = 1.92 × 1.92 cm, in-plane resolution 400 × 400 μm, and 6 coronal slices with slice thickness = 1 mm.

During the scan session of each rat, after 2 min baseline image acquisition, the stimulation was applied in 15 cycles, each consisting of 16 s of LH stimulation followed by 5 min of rest before the next cycle. Each block of 16-s stimulation consisted of eight 1-s trains of 1-ms 0.15-mA electrical current pulses delivered at 60, 120, or 200 Hz, separated by 1 s between trains. The 3 frequencies were applied in random order, with 5 repetitions of each frequency per experiment, for a total of 15 stimulus cycles. The stimulation paradigm used in conjunction with functional imaging was controlled through a customized program using LabVIEW software (National Instruments). To minimize potential radiofrequency artefacts, the stimulator cable was filtered with a 60-MHz low-pass filter (Mini-Circuits) before entering the MRI enclosure.

Dopamine-insensitive control experiments were performed as described above, except that 500 μM BM3h-WT protein was infused in place of 9D7. Additional experiments to record haemodynamic signals only were also performed with the same imaging and stimulation parameters, but in the absence of NAc cannula placement or intracranial contrast agent infusion.

Image analysis

Images were reconstructed using the PV 5.1 software and then imported into the AFNI software package (National Institute of Mental Health)[32] for further processing. High-resolution anatomical images of each rat were registered to a Waxholm coordinate space rat brain MRI atlas[33,34]. Functional imaging time series were preprocessed in steps that included slice timing correction, motion correction using a least-squares rigid-body volume registration algorithm, voxelwise intensity normalization, spatial smoothing with Gaussian spatial kernel of 0.5 mm full width at half maximum, and spatial resampling to double the image matrix size. Segmentation of brain from non-brain voxels was performed in MATLAB (MathWorks). Preprocessed time series were then co-registered onto the previously atlas-aligned anatomical images.

ROIs used for subsequent analyses were also defined with respect to standard rat atlases[33–35], and are described in Extended Data Fig. 7. Because of resolution differences between the atlas and the fMRI data, minor inaccuracies in the delineation of ROIs occur. Estimation of these so-called partial volume effects indicates that an average of 7% false-negative and 16% false-positive territory is included in each ROI.

T_1- and T_2*-weighted contributions to functional imaging data were extracted from the multi-echo image time series[36,37]. For each time point, T_1-weighted signals were defined by the image intensities obtained with TE = 4 ms. T_2*-weighted signals were defined by an independent component analysis of image intensity at all three echo times, from which components with strong TE dependence characteristic of BOLD contrast were identified and pooled using the multi-echo independent components analysis (ME-ICA) plugin to AFNI[38].

Stimulus-dependent T_1 and T_2*-weighted time courses were obtained using the 3dDeconvolve general linear modelling implementation in AFNI[32]. Lateral hypothalamus stimulus time blocks were used as event regressors. Six motion correction parameters from each rat were included as nuisance regressors, along with a linear baseline term. Outlier scans detected by median deviation from time series trends in each dataset were censored from the analysis. Stimulation-frequency-independent average responses were determined by using a single regressor to model medial forebrain bundle stimulation at all delivered frequencies. Frequency-dependent responses were determined in a separate calculation for which individual regressors for each stimulation frequency were used. Mean stimulus response functions of 288-s duration (corresponding to 36 image frames) were obtained in units of per cent signal change for each voxel in each rat. Per cent signal change maps were computed as the mean signal during the expected peak response time points 72–88 s (3 image frames) after stimulus onset, minus the baseline signal defined by the mean of response time points 8–48 s (5 frames) before stimulus onset. Per cent signal changes due to contrast agent infusion were calculated using the T_1-weighted MRI signal 50 min after injection minus the mean signal before injection, divided by the signal before injection. Unless otherwise noted, s.e.m. values associated with time courses, mean amplitudes and other response parameters were computed by jackknife resampling over multiple rats.

Quantitative analysis of dopamine concentrations

T_1-weighted fMRI signals can contain contributions from contrast agents (9D7 or BM3h-WT) and also from haemodynamic in-flow effects[39]. Our T_1-weighted fMRI data indeed displayed apparent flow-related signals of up to 3% in areas uninjected with contrast agent, a result consistent with previous experimental and modelling work[40–43]. Empirical investigation of the T_1-weighted fMRI results indicates that the apparent flow-related signals are sharply suppressed in brain areas that received doses of contrast agent sufficient to increase the baseline MRI signal by 5% or more (Fig. 1, Extended Data Fig. 2). This is probably a result of the shorter T_1 values in the injected tissue, compounded by microscopic heterogeneity in magnetic susceptibility induced by the presence of the contrast agent. Despite this suppression, mean stimulus-evoked T_1-weighted image time courses obtained in the presence of 9D7 and BM3h-WT proteins both retained a small positive response phase that peaked almost a minute after stimulus onset (Fig. 1d). This signal was echo time-dependent (Extended Data Fig. 3a), and probably reflects a residual haemodynamic contribution to the T_1-weighted fMRI signal. In addition, fMRI signals in the presence of 9D7, but not BM3h-WT, contained a negative signal phase closely associated with the stimulus and consistent with the expected turn-off of the 9D7 sensor in the presence of dopamine release.

To correct for the dopamine sensor-independent slow signal, we fit the T_1-weighted stimulus responses to a linear combination of two basis functions, one proportional to the mean T_1-weighted response obtained in the presence of BM3h-WT and the other proportional to a gamma distribution function with shape parameter $\alpha = 5.5$ and rate parameter $\beta = 0.54$, designed to emulate the fast response mediated by 9D7. Least-squares fitting was performed to determine the optimal contribution of each basis function to the stimulus response at each voxel in each rat, and the corrected response was taken to be the original response minus the contribution from the slowly varying term.

To verify the robustness of this baseline correction approach, we performed a second analysis in which baseline time courses were estimated independently for each rat using the ME-ICA algorithm. These baselines were then used for an analogous least-squares fitting and subtraction to generate corrected data for each voxel in each rat. Further analysis of these data indicate that the results are almost identical to those obtained using our initial approach involving basis functions (Extended Data Fig. 3b).

Corrected 9D7-mediated fMRI signal time courses were converted to estimated absolute dopamine concentrations using a quantitative

modelling approach introduced in previous work[4]. Dependence of T_1-weighted signal (S) on the local longitudinal relaxation rate (R_1) is given by the equation:

$$S = k \times \frac{\sin\alpha(1 - e^{-TR \times R_1})}{1 - \cos\alpha \times e^{-TR \times R_1}} \quad (1)$$

in which α is the flip angle (30°), TR is the repetition time (251.9 ms) and k is a constant of proportionality determined by proton density and instrument-dependent factors. R_1 is the longitudinal relaxation rate, given by:

$$R_1 = R_1^0 + M[\Theta \times r_1^{DA} + (1 - \Theta) \times r_1^{free}] \quad (2)$$

in which R_1^0 is the longitudinal relaxation rate of brain tissue in the absence of contrast agent (measured to be $0.31 \pm 0.01\ s^{-1}$)[4], M is the contrast agent concentration, r_1^{DA} ($0.10 \pm 0.00\ mM^{-1}\ s^{-1}$) and r_1^{free} ($0.83 \pm 0.01\ mM^{-1}\ s^{-1}$) are the relaxivities of 9D7 bound and not bound to dopamine, respectively. Θ is the fractional saturation of contrast agent, as a function of the contrast agent concentration M and dopamine concentration ([DA]), such that:

$$\Theta = \frac{[DA] + M + K_d - \sqrt{([DA] + M + K_d)^2 - 4[DA]M}}{2M} \quad (3)$$

in which $K_d = 1.3\ \mu M$ is the measured dissociation constant of 9D7 for dopamine[4,6,8]. Graphing of equation (2) for different values of M shows that S is approximately linear with dopamine concentrations up to over 30 μM for sensor concentrations of 40 μM or higher. This behaviour reflects the fact that changes in R_1 are small compared with the absolute R_1 in the brain, as well as the fact that concentrations of 9D7 present in the brain are well above the dopamine concentration and also well above the K_d for dopamine binding.

The analysis does not account for the kinetics of dopamine binding and unbinding to the sensor, but kinetic modelling of realistic dopamine fluctuations predicts that sensor binding behaviour closely tracks the equilibrium binding behaviour represented by equation (3), albeit in conjunction with perturbations to total dopamine kinetics (Extended Data Fig. 5).

According to equations (1) and (2), 40 μM 9D7 or BM3h-WT is sufficient to produce >5% baseline signal change in the absence of dopamine, which is also sufficient for apparently complete suppression of haemodynamic signals in the corrected T_1-weighted MRI data. For each rat that received a 9D7 infusion, voxels that experienced 5% or greater baseline change upon contrast agent injection were therefore identified, and stimulus-associated contrast changes in these voxels were interpreted as resulting from dopamine-binding to the contrast agent with a conversion factor of 8.0 μM per per cent signal change, as indicated by the graph in Extended Data Fig. 4a.

To quantify average dopamine release over multiple rats, the requirement for ≥5% baseline signal change due to contrast agent infusion was applied separately in each rat, dopamine concentrations were computed for each qualifying voxel in each rat and mean values over multiple rats were obtained for voxels for which data from three or more rats were available. To judge the robustness of topographic features in the dopamine maps, data from individual rats were normalized before averaging, yielding the maps in Extended Data Fig. 4d, with their accompanying s.e.m. values. The number of rats contributing to dopamine estimates at each position is indicated in Extended Data Figs. 4c, e.

Determination of dopamine-dependent impulse responses

To quantify the effect of dopamine release on BOLD fMRI signal changes, we performed a deconvolution analysis in MATLAB to determine the dopamine-dependent IRFs at each position for which both dopamine and BOLD data were available (Fig. 3). The calculation is mathematically analogous to the computation of mean dopamine and BOLD responses to LH stimulation, except that the input signal in this case is taken to be the dopamine response at each voxel, and the IRF at each point relates this dopamine input to the difference in BOLD signal in the absence minus the presence of treatment with D1 and D2 inhibitors, such that $[DA](t) \otimes IRF(t) = \Delta BOLD(t) + \varepsilon(t)$, in which ⊗ is the convolution operator and $\varepsilon(t)$ is an error term.

This equation is equivalent to the matrix equation $\mathbf{Dx} = \mathbf{b} + \boldsymbol{\varepsilon}$, in which each row of the matrix $\mathbf{D}$ contains dopamine amplitudes at time points t through $t + n - 1$, $\mathbf{x}$ is a vector of n coefficients containing n time points of the IRF, $\mathbf{b}$ is a vector containing the ΔBOLD data from time points n to t_{max}, the maximum time point acquired, and $\boldsymbol{\varepsilon}$ is a vector of $t_{max} - n + 1$ error terms. A linear least-squares solution to this problem is given by $\mathbf{x} = (\mathbf{D}^T\mathbf{D} + \lambda\mathbf{I})^{-1}\mathbf{D}^T\mathbf{b}$, in which $\mathbf{I}$ is the identity matrix and λ is a diagonal loading component set to 0.01, which addresses the problem of potential lack of invertibility of $\mathbf{D}^T\mathbf{D}$. The resulting IRF estimate embodied by $\mathbf{x}$ is thus completely data-driven and does not use a closed form or make corresponding assumptions.

The calculations were implemented in MATLAB and performed on each voxel individually. IRFs from individual voxels were averaged to obtain ROI means, and error bars were obtained by performing jackknife resampling over BOLD datasets. BOLD and dopamine imaging data for this analysis were obtained under identical experimental conditions but from different groups of rats because of the attenuating effect of the dopamine sensor on local haemodynamic signals.

Neurochemical functional connectivity analyses

Correspondence between mean striatal dopamine and global BOLD signals was computed using the 3dDeconvolve multiple regression function in AFNI. To identify brain regions with average BOLD time courses that corresponded most closely to striatal dopamine time courses (Fig. 4a, b), two regressors were defined: (1) a striatal dopamine regressor was obtained by concatenating the mean dopamine responses to 60-Hz, 120-Hz, and 200-Hz LH stimulation, each averaged over five 9D7-injected rats and voxels in the NAc; and (2) a mean BOLD signal regressor was defined by concatenating the mean BOLD responses at each stimulus frequency, in each case averaged over the entire imaging FOV in all uninjected rats (Extended Data Fig. 7). The degree of dopamine tracking in each voxel was defined by the regression coefficient assigned to the dopamine response regressor, and the statistical significance of dopamine tracking was assessed according to an F-test.

To assess covariation of BOLD and dopamine signals across multiple individual rats for which simultaneous striatal dopamine and distal BOLD fMRI data were available (Fig. 4c, d), a second regression analysis was performed, in which mean stimulus-dependent dopamine responses for each striatal voxel for which data from three or more rats were available were concatenated over rats and interpreted in terms of mean BOLD signal in select distal ROIs in the same rats. The resulting maps of regression coefficients in contrast-agent-filled striatal voxels indicate the extent to which BOLD signals in the distal ROIs correspond with local dopamine signals in each of the striatal voxels. This analysis approach was also used to examine functional connectivity between NAc dopamine signals in the absence versus presence of systemic inhibition of D1 and D2 receptors with SCH 23390 and eticlopride, as specified in 'Receptor inactivation treatments' (Extended Data Fig. 9).

Amperometry recordings

For comparison with dopamine-dependent fMRI results, dopamine time courses were recorded using fixed potential amperometry, under conditions matched to those used for imaging (Extended Data Fig. 5a). Rats were sedated with medetomidine, paralyzed with pancuronium and mechanically ventilated as for MRI. In each subject, a bipolar stimulation electrode was lowered into LH (anterioposterior −2.8 mm, mediolateral +1.7 mm, dorsoventral +8.6 mm). A carbon fibre recording

electrode, 7-μm diameter with about 1-mm exposed tip length, was lowered to the centre of the NAc (anterioposterior +1.5 mm, mediolateral +1.5 mm, dorsoventral +7.4 mm). An Ag/AgCl reference electrode was implanted at surface of the brain contralateral to the carbon fibre electrode. A Picostat and an eCorder system from eDAQ were used for data acquisition. A fixed potential of 0.8 V was applied to the recording electrode and the oxidation current was continuously monitored with 10-kHz sampling. Once a stable baseline was achieved, LH stimulation was performed using parameters again identical to MRI conditions, and amperometry data were recorded throughout. Following each recording, the carbon fibre electrode was removed from the brain and calibrated in a custom-made flow cell, using dopamine concentrations of 0–10 μM in the presence of 600 μM ascorbic acid. A calibration constant of 0.30 ± 0.11 nA/μM dopamine (mean ± s.d., $n = 3$) was obtained.

General statistical methods

Comparisons of mean fMRI amplitudes, durations and regression coefficients were performed using Student's *t*-test. The significance of regressor-dependent contributions in general linear model analyses, including assessment of the proportionality between dopamine and BOLD signals, was evaluated using the *F*-test. Differences between correlation coefficients were evaluated using Fisher's *Z*-test. All numerical results are expressed in the form of mean ± s.e.m., unless otherwise specified. All quantitative data analyses were performed using AFNI and MATLAB.

Reporting summary

Further information on research design is available in the Nature Research Reporting Summary linked to this paper.

Data availability

The datasets generated and analysed in the current study are available from the corresponding author upon reasonable request. Source Data for Figs. 2–4 are provided with the paper.

Code availability

Custom code is available from the corresponding author upon reasonable request.

28. Koerber, J., Goodman, D., Barnes, J. L. & Grimm, J. W. The dopamine D2 antagonist eticlopride accelerates extinction and delays reacquisition of food self-administration in rats. *Behav. Pharmacol.* **24**, 633–639 (2013).
29. Verty, A. N., McGregor, I. S. & Mallet, P. E. The dopamine receptor antagonist SCH 23390 attenuates feeding induced by Δ^9-tetrahydrocannabinol. *Brain Res.* **1020**, 188–195 (2004).
30. Calaminus, C. & Hauber, W. Intact discrimination reversal learning but slowed responding to reward-predictive cues after dopamine D1 and D2 receptor blockade in the nucleus accumbens of rats. *Psychopharmacology (Berl.)* **191**, 551–566 (2007).
31. Lex, A. & Hauber, W. Dopamine D1 and D2 receptors in the nucleus accumbens core and shell mediate Pavlovian-instrumental transfer. *Learn. Mem.* **15**, 483–491 (2008).
32. Cox, R. W. AFNI: software for analysis and visualization of functional magnetic resonance neuroimages. *Comput. Biomed. Res.* **29**, 162–173 (1996).
33. Papp, E. A., Leergaard, T. B., Calabrese, E., Johnson, G. A. & Bjaalie, J. G. Waxholm Space atlas of the Sprague Dawley rat brain. *Neuroimage* **97**, 374–386 (2014).
34. Papp, E. A., Leergaard, T. B., Calabrese, E., Johnson, G. A. & Bjaalie, J. G. Addendum to "Waxholm Space atlas of the Sprague Dawley rat brain" [NeuroImage 97 (2014) 374-386]. *Neuroimage* **105**, 561–562 (2015).
35. Paxinos, G. & Watson, C. *The Rat Brain in Stereotaxic Coordinates* Compact 6th Edn (Academic, 2009).
36. Kundu, P., Inati, S. J., Evans, J. W., Luh, W. M. & Bandettini, P. A. Differentiating BOLD and non-BOLD signals in fMRI time series using multi-echo EPI. *Neuroimage* **60**, 1759–1770 (2012).
37. Peltier, S. J. & Noll, D. C. T. T_2* dependence of low frequency functional connectivity. *Neuroimage* **16**, 985–992 (2002).
38. Kundu, P., Santin, M. D., Bandettini, P. A., Bullmore, E. T. & Petiet, A. Differentiating BOLD and non-BOLD signals in fMRI time series from anesthetized rats using multi-echo EPI at 11.7 T. *Neuroimage* **102**, 861–874 (2014).
39. Frahm, J., Merboldt, K. D., Hänicke, W., Kleinschmidt, A. & Boecker, H. Brain or vein—oxygenation or flow? On signal physiology in functional MRI of human brain activation. *NMR Biomed.* **7**, 45–53 (1994).
40. Frahm, J., Merboldt, K. D. & Hänicke, W. Functional MRI of human brain activation at high spatial resolution. *Magn. Reson. Med.* **29**, 139–144 (1993).
41. Kim, S. G., Hendrich, K., Hu, X., Merkle, H. & Uğurbil, K. Potential pitfalls of functional MRI using conventional gradient-recalled echo techniques. *NMR Biomed.* **7**, 69–74 (1994).
42. Diemling, M., Barth, M. & Moser, E. Quantification of signal changes in gradient recalled echo FMRI. *Magn. Reson. Imaging* **15**, 753–762 (1997).
43. Wang, X., Zhu, X. H., Zhang, Y. & Chen, W. Large enhancement of perfusion contribution on fMRI signal. *J. Cereb. Blood Flow Metab.* **32**, 907–918 (2012).

Acknowledgements This research was funded by National Institutes of Health grants R01 DA038642 and U01 NS103470 to A.J. N.L. was supported by a Stanley Fahn Research Fellowship from the Parkinson's Disease Foundation. The authors thank T. Lee and L. Cai for initial assistance with the experimental methods; P. Bandettini for advice with multi-echo MRI acquisition; and A. Graybiel, S. Lall and I. Witten for comments on the data and manuscript.

Author contributions N.L. and A.J. designed the research, interpreted the results and wrote the paper. N.L. conducted all of the experiments and analysed the data.

Competing interests The authors declare no competing interests.

Additional information

Supplementary information is available for this paper at https://doi.org/10.1038/s41586-020-2158-3.

Correspondence and requests for materials should be addressed to A.J.

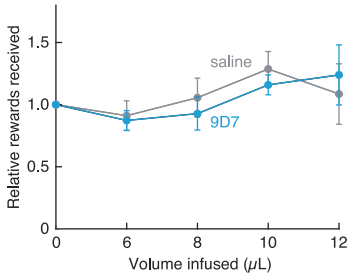

Extended Data Fig. 1 | Intracranial self-stimulation in the presence and absence of 9D7. Behaviourally shaped rats implanted with unilateral cannulae targeting the ventral striatum performed intracranial self-stimulation during continuous injection of 500 μM of the dopamine sensor 9D7 (blue) or saline vehicle (grey), under infusion conditions used for imaging experiments. The number of rewards received per trial is graphed, relative to rewards received before infusion, showing no significant difference between infusion of 9D7 versus saline. Error bars denote s.e.m. of data from $n = 5$ rats each.

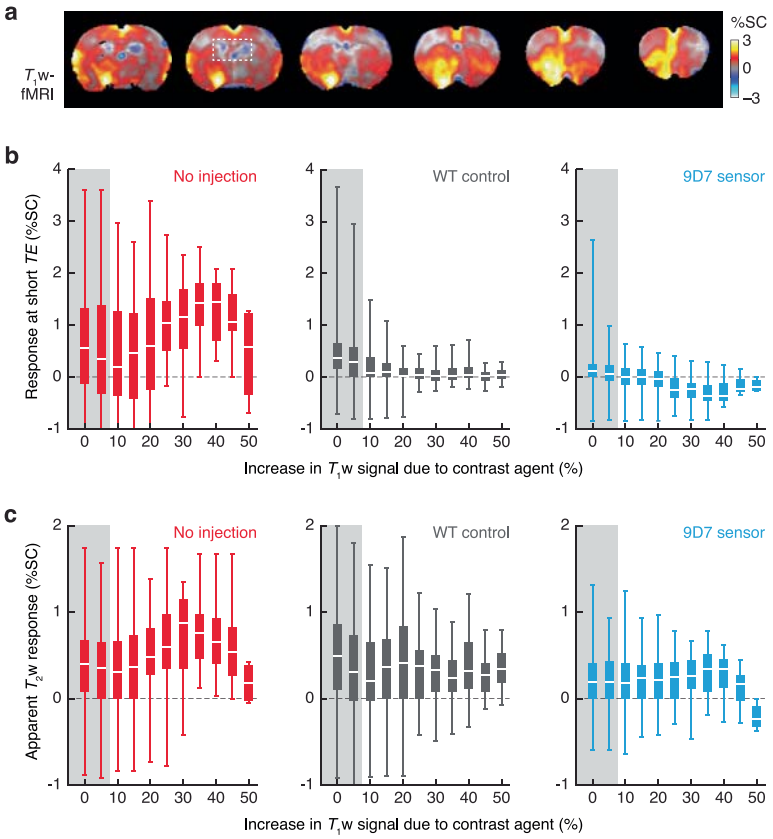

Extended Data Fig. 2 | Suppression of haemodynamic signals by contrast agents infused into the ventral striatum. a, T_1-weighted fMRI data from uninjected rats. Mean T_1-weighted responses to LH stimulation from five rats that were not injected with MRI contrast agents, measured under conditions identical to those used for the injected rats in Fig. 1b. Negative haemodynamic signals in the ventricles are apparent (dotted box). **b**, Striatal voxels were scored on the basis of the T_1-weighted signal change that they experienced following 50 min of contrast agent infusion (9D7 dopamine sensor or BM3h-WT control protein). Uninjected rats were given a pseudo-score on the basis of the signal change experienced by spatially equivalent voxels in rats injected with 9D7. Box plots show T_1-weighted responses evoked by LH stimulation over all voxels as a function of the injection score, in 5% bins, for uninjected rats (left), rats that received infusion of BM3h-WT protein (middle) and rats that received 9D7 (right). Grey shading indicates bins excluded from molecular imaging analysis owing to incomplete suppression of haemodynamic responses. **c**, Graphs equivalent to those shown in **b** showing the variation of T_2*-weighted signal obtained using multi-echo analysis, as a function of injected contrast agent dose for injected rats or a pseudo-dose for uninfused rats. All box plots indicate median (white line), first and third quartiles (box), and full data ranges (whiskers) over voxels in each bin. Individual voxel intensities are means over five rats in each condition.

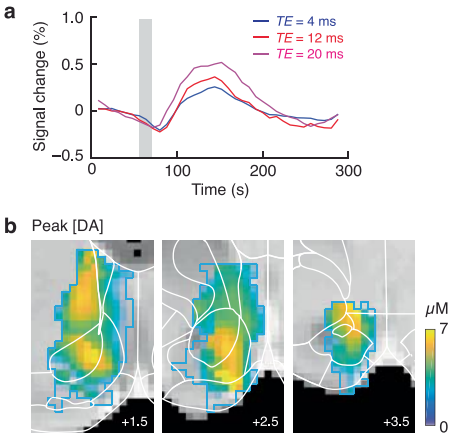

Extended Data Fig. 3 | Baseline correction of dopamine fMRI data using T_2*-dependent signals. a, Echo time dependence of the slow component of the fMRI signal recorded in the presence of the 9D7 dopamine sensor in the ventral striatum. Variation of the slow positive signal with TE provides a basis for extracting the baseline time course using the ME-ICA approach. Error margins are omitted for graphical clarity. **b**, Quantitative maps of dopamine release formed after baseline correction using the ME-ICA signal. Features correspond closely to the maps in Fig. 2a, which were corrected using a baseline derived from the control BM3h-WT T_1-weighted fMRI data, indicating that the choice of baseline correction method makes little difference to the outcome.

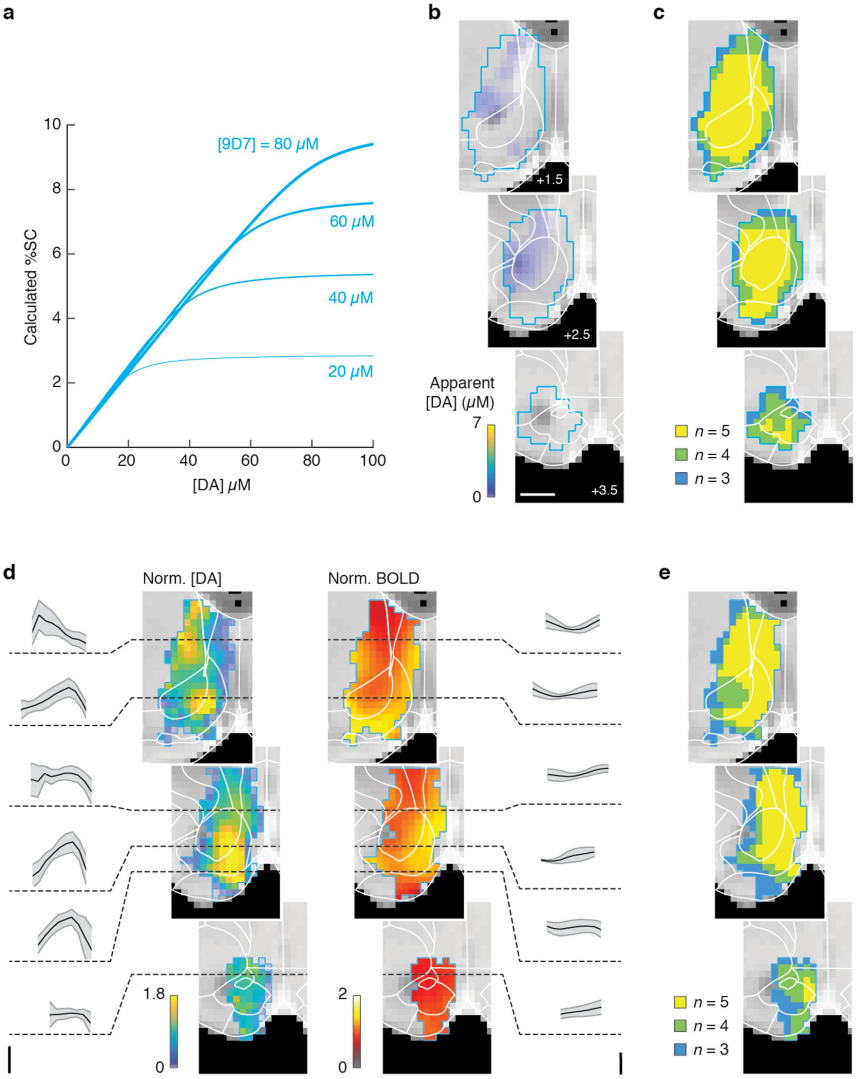

Extended Data Fig. 4 | Quantification of dopamine concentrations. a, MRI per cent signal changes (%SC) as a function of dopamine concentration ([DA]) were estimated with respect to [DA] = 0 μM from the in vitro relaxivity of 9D7 and experimental parameters used in the imaging. **b**, To verify the absence of baseline contributions to dopamine maps obtained with 9D7, mock dopamine imaging was performed using the BM3h-WT control contrast agent. Signal changes induced by LH stimulation were observed in rats injected with the dopamine-insensitive contrast agent BM3h-WT, and mock dopamine maps were computed as described in 'Quantitative analysis of dopamine concentrations' for molecular imaging experiments using the 9D7 sensor. Scale bar, 1 mm. **c**, Number of rats contributing to data from each voxel in **b**. The results show that minimal dopamine concentrations were observed, indicating effective suppression of background or nonspecific signals to the T_1-weighted data. **d**, Robustness of spatial features in dopamine and BOLD fMRI response maps was verified by examining average data across rats. Dopamine release or BOLD fMRI amplitudes from each individual rat that contributed to Fig. 2a, b were normalized to the mean response level and standard errors were computed to determine error margins, shown in grey shading in the cross-sections shown on the left (for dopamine) and right (for BOLD). These data indicate that the locations of peak dopamine responses in the ventromedial striatum are conserved among rats, whereas the BOLD responses are relatively uniform across the FOV. Scale bars correspond to 3 μM dopamine (left) and 1% BOLD signal modulation (right), before normalization. **e**, The number of rats contributing to each voxel of the dopamine data averages in **d**, as well as Fig. 2.

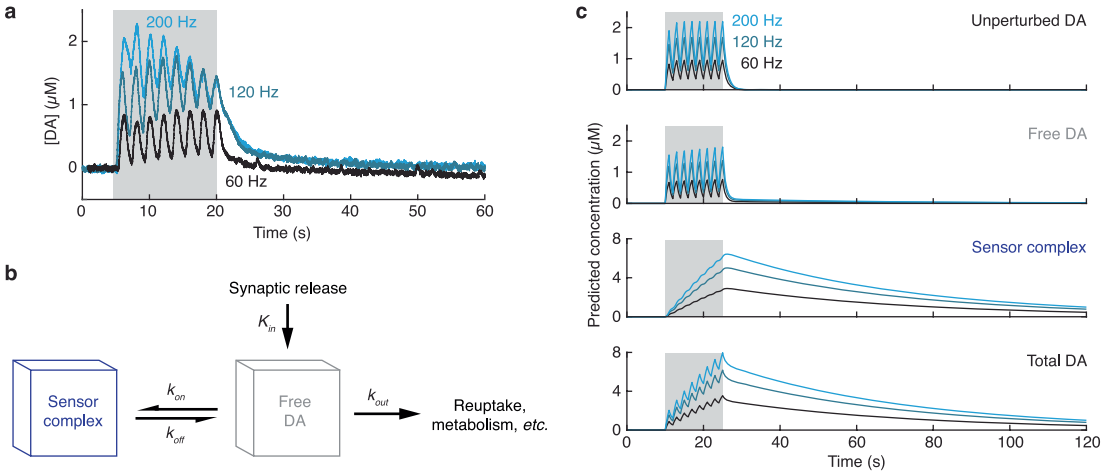

Extended Data Fig. 5 | Imaging-independent estimation of dopamine release dynamics. a, Amperometric recording was used to measure dopamine release elicited by LH stimulation. Lateral hypothalamus stimulation at 60-, 120- and 200-Hz frequencies was performed in medetomidine-sedated rats prepared in the same way as for functional imaging experiments. Amperometric recordings of a representative rat were obtained using carbon fibres calibrated after in vivo recording to obtain absolute measurements of dopamine concentration. **b**, Diagram of a kinetic model that accounts for the introduction of dopamine by synaptic release at the fixed rate K_{in} during stimulation, interconversion of free and 9D7-bound dopamine with rate constants k_{on} and k_{off}, and removal of free dopamine with the rate constant k_{out}. **c**, Simulations were performed using parameters chosen to emulate the amperometry data in the absence of 9D7, with K_{in} = 1.3, 2.3 and 3 μM s^{-1}—corresponding to the three stimulus intensities of 60, 120 and 200 Hz, respectively—and a k_{out} value of 1 s^{-1}. Values of k_{on} (0.013 $\mu M^{-1} s^{-1}$) and k_{off} (0.03 s^{-1}) were derived from stopped flow binding data and empirical estimates of dopamine removal rate reported in a previous publication[4]. The top trace shows simulated free dopamine concentration in the absence of 9D7 (unperturbed dopamine), and the second trace from the top shows simulated free dopamine in the presence of 40 μM 9D7, revealing a modest buffering effect. The bottom two traces depict the simulated sensor complex concentration in the presence of 40 μM 9D7, as well as the total dopamine concentration under these conditions. These results reveal the expected broadening of total dopamine kinetics in the presence of the 9D7 sensor, but also show that the sensor complex concentration closely tracks total dopamine levels in the system.

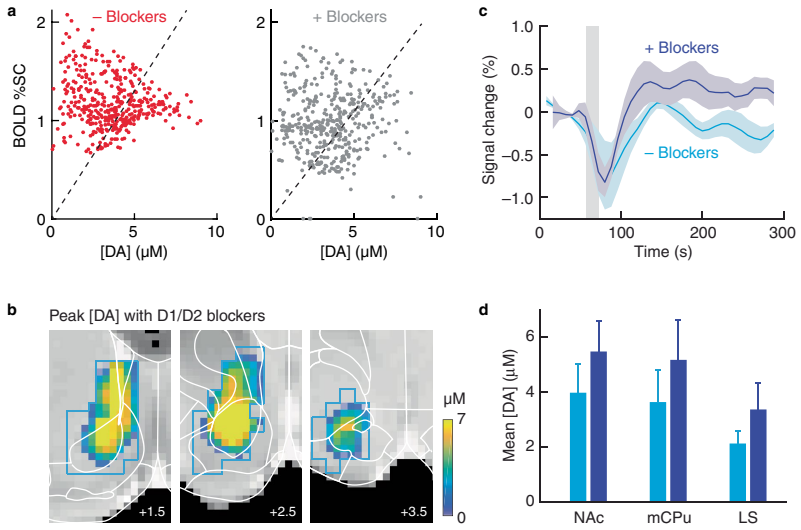

Extended Data Fig. 6 | Additional effects of dopamine receptor inhibition. **a**, Scatter plots display the effects of dopamine inhibitors on the correspondence of mean dopamine concentration ([DA]) and BOLD amplitudes (%SC) evoked by LH stimulation. Each dot denotes one voxel in the absence of dopamine receptor blockers (left), or in the presence of SCH 23390 and eticlopride (right). Dashed lines indicate best-fit line of proportionality between the two measures. The addition of D1 and D2 receptor blockers significantly improved the correspondence (F-test $P = 0.0019$). **b**, Dopamine inhibition exerts a negligible effect on dopamine release per se. The 9D7 sensor was infused into the ventral striatum as for experiments in Figs. 1, 2, and multigradient imaging was performed to acquire fMRI data in the presence of systemic SCH 23390 and eticlopride treatment. Maps of peak dopamine release computed as in the experiments of Fig. 2a reveal a distribution that corresponds closely to results in the absence of blockers, albeit with somewhat different spatial coverage (cyan outline) due to infusion variability among rats. Coordinates with respect to bregma are noted in the bottom right of each coronal slice. **c**, Mean time courses of NAc dopamine observed in the absence (cyan) and presence (dark blue) of treatment with D1 and D2 blockers. Shading denotes s.e.m. of five rats (– blockers) or four rats (+ blockers). **d**, Comparison of mean peak dopamine-release amplitudes in absence (cyan) versus presence (dark blue) of D1 and D2 inhibitors, over three striatal regions for which data were obtained in both conditions. Error bars denote s.e.m. All differences were not significant with t-test $P \geq 0.07$.

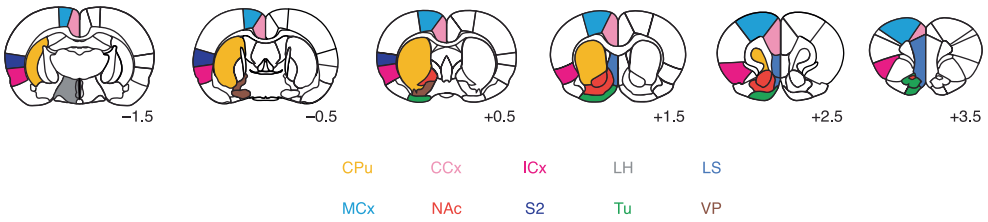

Extended Data Fig. 7 | ROIs used in brain-wide functional connectivity analysis. Relevant ROIs were defined with respect to standard brain atlases and are shown here colour-coded by region: caudate-putamen (CPu), cingulate cortex (CCx), insular cortex (ICx), lateral hypothalamus (LH), lateral septal area (LS), motor cortex (MCx), nucleus accumbens (NAc), olfactory tubercle (Tu), secondary somatosensory cortex (S2) and ventral pallidum (VP). Coordinates of each slice relative to bregma are indicated. Voxel-level definitions of the LS, NAc, Tu and medial CPu are specified in Fig. 2d, and account for experimentally determined anatomical landmarks in the ventral striatum, as reflected in the MRI data.

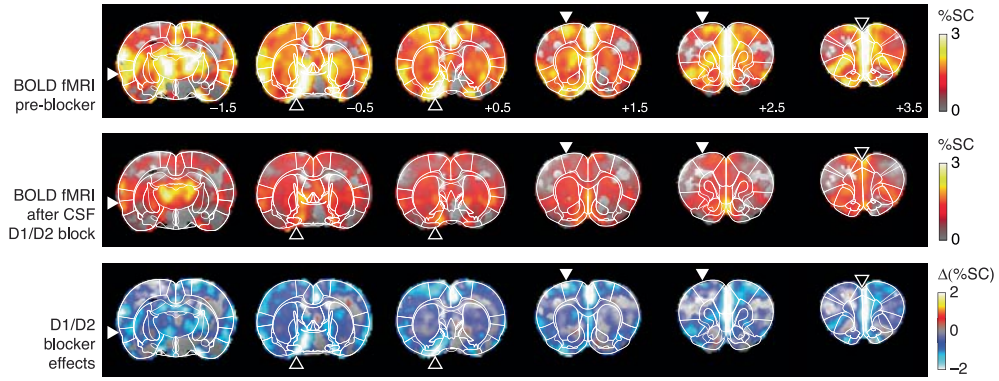

Extended Data Fig. 8 | Effect of intracerebrospinal fluid administration of D1 and D2 inhibitors on reward-induced brain activation. Three rats were implanted with a cannula targeting the cerebrospinal fluid (CSF) at the cisterna magna and imaged during rewarding stimulation of LH. Maps show per cent signal change (%SC) before (top) and after (middle) infusion of a cocktail containing SCH 23390 and eticlopride, both for voxels with significant activation in the pre-blocker condition ($P \leq 10^{-5}$). The bottom row shows the corresponding difference signal map. Labels in the top panel denote coordinates with respect to bregma. Filled arrowheads denote areas of reduced activation in the ICx and S2 region (−1.5 mm) and in MCx (+1.5 and +2.5 mm) observed upon dopamine receptor blockade and similar to effects observed with systemic inhibition treatment in Fig. 4a. Open arrowheads denote differences from the systemic treatment results along the midline (+3.5 mm) and in ventral areas (−0.5 and +0.5 mm) that probably received much higher doses of the inhibition cocktail owing to their proximity to the CSF infusion route.

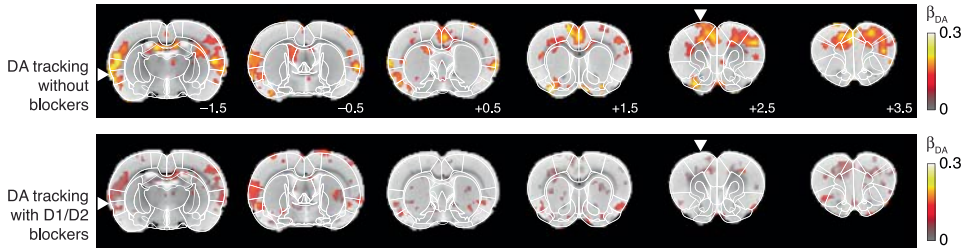

Extended Data Fig. 9 | Functional connectivity between striatal dopamine and distal BOLD signals before and after dopamine receptor blockade. Regression analysis was used to determine the amplitude of dopamine-tracking signals (β_{DA}, F-test $P \leq 0.05$) observed throughout the brain in regions distal to 9D7 infusion sites in the ventral striatum using the same methods as for experiments shown in Fig. 4c, d. The analysis was performed on two groups of rats, one untreated with SCH 23390 and eticlopride (top) ($n = 5$) and one pre-treated with the cocktail of systemic D1 and D2 inhibitors ($n = 4$). In each case, dopamine and BOLD data were obtained from the same rats, and β_{DA} values reflect the shared variance of simultaneously acquired, temporally varying dopamine and BOLD signals across multiple individuals. Labels in the top panel denote coordinates with respect to bregma. Arrowheads highlight areas in which blockade of the D1 and D2 receptors substantially reduces tracking behaviour in the MCx (+2.5 mm) and in ICx and S2 (−1.5 mm).

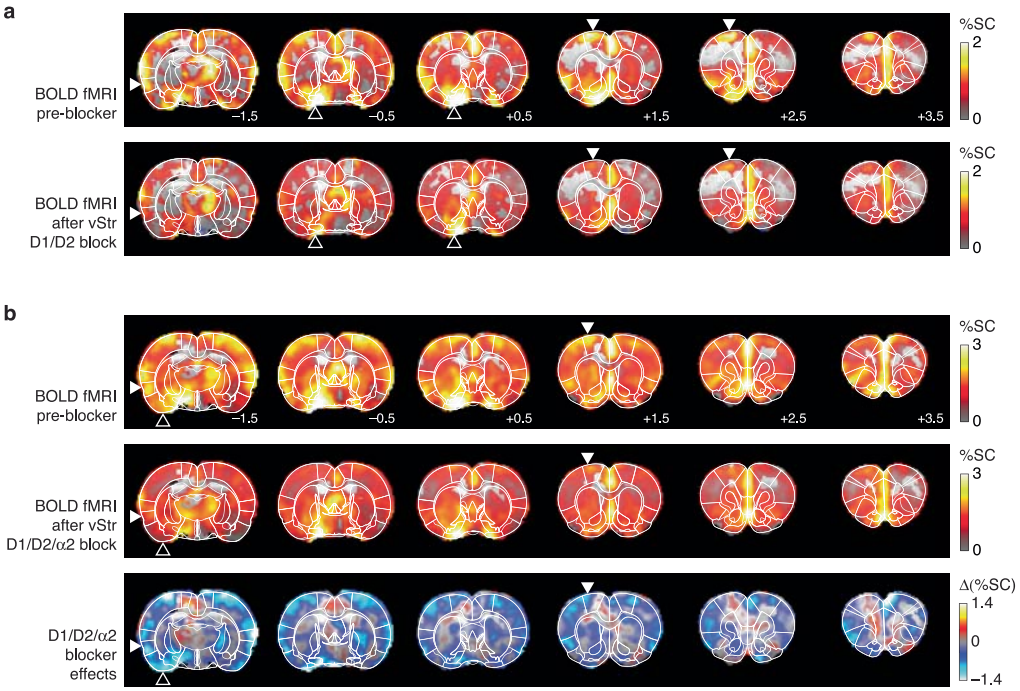

Extended Data Fig. 10 | Effect of ventral-striatal receptor blockade on reward-induced brain activation. a, D1 and D2 inhibitors were intracranially infused into five rats implanted with cannulae targeting the ventral striatum, and imaged during rewarding LH stimulation. Maps show per cent signal change (%SC) before (top) and after (middle) administration of a cocktail containing SCH 23390 and eticlopride, both for voxels with significant activation in the pre-blocker condition ($P \leq 10^{-5}$). The corresponding difference map is presented in Fig. 4e. Labels in the top panel denote coordinates with respect to bregma. Filled arrowheads denote areas of highly reduced activation in the ICx (−1.5 mm) and MCx (+1.5 and +2.5 mm) observed upon local blockade of the D1 and D2 receptors. Reduced activation in the Tu and ventral pallidum (open arrowheads) probably reflects direct effects of the locally infused dopamine blockers. **b**, A combination of dopamine inhibitors and a noradrenaline inhibitor was intracranially infused into four rats implanted with cannulae targeting the ventral striatum (vStr), and imaged during rewarding stimulation of LH. Maps show per cent signal change (%SC) before (top) and after (middle) infusion of a cocktail containing SCH 23390, eticlopride and the α2 receptor antagonist yohimbine, both for voxels with significant activation in the pre-blocker condition ($P \leq 10^{-5}$). The bottom row shows the corresponding difference signal map. Filled arrowheads at bregma −1.5 and +1.5 denote areas at the intersection of ICx and S2, and also in MCx, in which the reduction of the BOLD signal parallels effects observed with blockade of the D1 and D2 receptors alone (**a**, Fig. 4e). Open arrowhead at bregma −1.5 mm indicates an amygdalar region that may be sensitive to the addition of yohimbine in the treatment mixture.

nature research

Corresponding author(s): Alan Jasanoff

Last updated by author(s): Jan 15, 2020

Reporting Summary

Nature Research wishes to improve the reproducibility of the work that we publish. This form provides structure for consistency and transparency in reporting. For further information on Nature Research policies, see Authors & Referees and the Editorial Policy Checklist.

Statistics

For all statistical analyses, confirm that the following items are present in the figure legend, table legend, main text, or Methods section.

n/a	Confirmed	
☐	☒	The exact sample size (*n*) for each experimental group/condition, given as a discrete number and unit of measurement
☐	☒	A statement on whether measurements were taken from distinct samples or whether the same sample was measured repeatedly
☐	☒	The statistical test(s) used AND whether they are one- or two-sided *Only common tests should be described solely by name; describe more complex techniques in the Methods section.*
☒	☐	A description of all covariates tested
☐	☒	A description of any assumptions or corrections, such as tests of normality and adjustment for multiple comparisons
☐	☒	A full description of the statistical parameters including central tendency (e.g. means) or other basic estimates (e.g. regression coefficient) AND variation (e.g. standard deviation) or associated estimates of uncertainty (e.g. confidence intervals)
☐	☒	For null hypothesis testing, the test statistic (e.g. *F*, *t*, *r*) with confidence intervals, effect sizes, degrees of freedom and *P* value noted *Give P values as exact values whenever suitable.*
☒	☐	For Bayesian analysis, information on the choice of priors and Markov chain Monte Carlo settings
☒	☐	For hierarchical and complex designs, identification of the appropriate level for tests and full reporting of outcomes
☐	☒	Estimates of effect sizes (e.g. Cohen's *d*, Pearson's *r*), indicating how they were calculated

Our web collection on statistics for biologists contains articles on many of the points above.

Software and code

Policy information about availability of computer code

Data collection	Paravision 5.1 (Bruker), eDAQ
Data analysis	AFNI (NIH), MATLAB (Mathworks); scripts used for data analysis are available upon reasonable request.

For manuscripts utilizing custom algorithms or software that are central to the research but not yet described in published literature, software must be made available to editors/reviewers. We strongly encourage code deposition in a community repository (e.g. GitHub). See the Nature Research guidelines for submitting code & software for further information.

Data

Policy information about availability of data

All manuscripts must include a data availability statement. This statement should provide the following information, where applicable:

- Accession codes, unique identifiers, or web links for publicly available datasets
- A list of figures that have associated raw data
- A description of any restrictions on data availability

The datasets generated and analysed in the current study are available from the corresponding author upon reasonable request.

Field-specific reporting

Please select the one below that is the best fit for your research. If you are not sure, read the appropriate sections before making your selection.

☒ Life sciences ☐ Behavioural & social sciences ☐ Ecological, evolutionary & environmental sciences

For a reference copy of the document with all sections, see nature.com/documents/nr-reporting-summary-flat.pdf

Life sciences study design

All studies must disclose on these points even when the disclosure is negative.

Sample size	Sample sizes are noted in each case.
Data exclusions	Only experimental sessions that were prematurely terminated due to major technical failures were excluded from analysis.
Replication	All experiments were performed with multiple replicates, and standard statistical methods were used to accept or reject null hypotheses of no effect.
Randomization	N/A
Blinding	N/A

Reporting for specific materials, systems and methods

We require information from authors about some types of materials, experimental systems and methods used in many studies. Here, indicate whether each material, system or method listed is relevant to your study. If you are not sure if a list item applies to your research, read the appropriate section before selecting a response.

Materials & experimental systems

n/a	Involved in the study
☒	☐ Antibodies
☒	☐ Eukaryotic cell lines
☒	☐ Palaeontology
☐	☒ Animals and other organisms
☒	☐ Human research participants
☒	☐ Clinical data

Methods

n/a	Involved in the study
☒	☐ ChIP-seq
☒	☐ Flow cytometry
☐	☒ MRI-based neuroimaging

Animals and other organisms

Policy information about studies involving animals; ARRIVE guidelines recommended for reporting animal research

Laboratory animals	Male Sprague-Dawley rats (300-350 g)
Wild animals	The study did not involve wild animals.
Field-collected samples	The study did not involve sampled collected from the field.
Ethics oversight	All procedures were performed in strict compliance with US Federal guidelines, with oversight by the MIT Committee on Animal Care.

Note that full information on the approval of the study protocol must also be provided in the manuscript.

Magnetic resonance imaging

Experimental design

Design type	block design
Design specifications	During each animal's scan session, after 2 mins baseline image acquisition, the stimulation was applied in 15 cycles, each consisting of 16 s stimulation followed by 5 min of rest before the next cycle. Each block of 16 s stimulation consisted of eight 1 s trains of 1 ms 0.15 mA electrical current pulses delivered at 60, 120, or 200 Hz, separated by 1 s between trains. The three frequencies were applied in random order, with five repetitions of each frequency per experiment, for a total of 15 stimulus cycles.
Behavioral performance measures	To assess the ability of the implanted LH electrodes to support rewarding stimulation, rats were evaluated for intracranial self-stimulation (ICSS) behavior. A minimum of 2 s was required between the onsets of successive nose poke-triggered rewards. ICSS was quantified over three 30 s trial periods in each animal prior to imaging.

Acquisition

Imaging type(s): Functional and structural

Field strength: 9.4 T

Sequence & imaging parameters: Functional image series were acquired using a multi-gradient echo pulse sequence with bandwidth = 200 kHz, TE values = 4, 12, and 20 ms, FA = 30, TR = 251.9 ms, scan time = 8 s, FOV = 1.92 x 1.92 cm, in-plane resolution 400 x 400 µm, and 6 coronal slices with slice thickness = 1 mm. High resolution anatomical MRI images were acquired using a T2-weighted rapid acquisi-tion with refocused echoes (RARE) pulse sequence with RARE factor = 8, effective TE = 30 ms, TR = 5 s, FOV = 1.92 x 1.92 cm, in plane resolution 100 µm x 100 µm, and slice thickness = 1 mm for six coronal slices.

Area of acquisition: Six coronal brain slices ranging from Bregma -1.5 mm to +3.5 mm were imaged. These are the brain regions anterior to the stimulation site (Bregma -2.9 mm) on LH, and the location where SNR of the images are not affected by the implantation of the stimulation electrode.

Diffusion MRI ☐ Used ☒ Not used

Preprocessing

Preprocessing software: Functional imaging time series were preprocessed using AFNI in steps that included slice timing correction, motion correction using a least squares rigid-body volume registration algorithm, voxel-wise intensity normalization, spatial smoothing with Gaussian spatial kernel of 0.5 mm full width at half maximum, and spatial resampling to double the image matrix size. Segmentation of brain from non-brain voxels was performed in MATLAB (Mathworks).

Normalization: High-resolution anatomical images of each animal were registered to a Waxholm coordinate space rat brain MRI atlas. Preprocessed time series were then co-registered onto the previously atlas-aligned anatomical images. Linear transformation 3dAllineate in AFNI was used for registration with the cost function of Local Pearson Correlation Abs (LPA) and/or Least Squares (LS) .

Normalization template: The template used for normalization/registration is the Waxholm coordinate space rat brain MRI atlas. ROIs were defined with respect to Paxinos and Waxholm atlases.

Noise and artifact removal: AFNI functions were used for motion correction, and also censor time points that contain too much motion.

Volume censoring: Outlier scans detected by median deviation from time series trends in each data set were censored from the analysis, using functions implemented in AFNI.

Statistical modeling & inference

Model type and settings: Comparisons of mean fMRI amplitudes, durations, and regression coefficients were performed using Student's t-test. Significance of regressor-dependent contributions in GLM analyses, including assessment of the proportionality between dopamine and BOLD signals, was evaluated using F-test. Differences between correlation coefficients were evaluated us-ing Fisher's Z-test.

Effect(s) tested: Responses to 60 Hz, 120 Hz, and 200 Hz stimulation of LH were assessed by dopamine and hemodynamic fMRI, both before and after treatment with inhibitors of dopamine receptors.

Specify type of analysis: ☐ Whole brain ☐ ROI-based ☒ Both

Anatomical location(s): High-resolution anatomical images of each animal were registered to a Waxholm coordinate space rat brain MRI atlas. ROIs used for subsequent analyses were defined with respect to Waxholm and Paxinos rat atlases.

Statistic type for inference (See Eklund et al. 2016): Voxel-wise, ROI-wise

Correction: Statistical thresholds noted throughout.

Models & analysis

n/a	Involved in the study
☐	☒ Functional and/or effective connectivity
☒	☐ Graph analysis
☒	☐ Multivariate modeling or predictive analysis

Functional and/or effective connectivity: Linear regression